Hexagonal Ge Grown by Molecular Beam Epitaxy on Self-Assisted GaAs Nanowires

Iuliia Dudko, Thomas Dursap, Anne Lamirand, Claude Botella, Philippe Regreny, Alexandre Danescu, Solène Brottet, Matthieu Bugnet, Sumeet Walia, Nicolas Chauvin, et al.

Hexagonal Ge grown by molecular beam epitaxy on self-assisted GaAs nanowires

Iuliia Dudko[1,2,3], Thomas Dursap[1], Anne D. Lamirand[1], Claude Botella[1], Philippe Regreny[1], Alexandre Danescu[1], Solène Brottet[1], Matthieu Bugnet[2], Sumeet Walia[2,3], Nicolas Chauvin[1], José Penuelas[1]*

[1] Univ Lyon, Ecole Centrale de Lyon, CNRS, INSA Lyon, Université Claude Bernard Lyon 1, CPE Lyon, INL, UMR 5270, 69130 Ecully, France

[2] School of Engineering, RMIT University, Melbourne 3001, Victoria, Australia

[3] Functional Materials and Microsystems, Research Group and Micro Nano Research Facility, RMIT University, Melbourne 3001, Victoria, Australia

[4] Univ Lyon, CNRS, INSA Lyon, UCBL, MATEIS, UMR 5510, 69621 Villeurbanne, France

[*] To whom correspondence should be addressed. E-mail : jose.penuelas@ec-lyon.fr

Abstract: Hexagonal group IV materials like silicon and germanium are expected to display remarkable optoelectronic properties for future development of photonic technologies. However, the fabrication of hexagonal group IV semiconductors within the vapor-liquid-solid method has been obtained using gold as a catalyst thus far. In this letter, we show the synthesis of hexagonal Ge on self-assisted GaAs nanowires using molecular beam epitaxy. With an accurate tuning of the Ga and As molecular beam flux we selected the crystal phase, cubic or hexagonal, of the GaAs NWs during the growth. A 500 nm-long hexagonal segment of Ge with high structural quality and without any visible defects is obtained, and we show that Ge keeps the crystal phase of the core using scanning transmission electron microscopy. Finally X-ray Photoelectron Spectroscopy reveals a strong incorporation of As in the Ge. This study demonstrates the first growth of hexagonal Ge in the Au-free approach, integrated on silicon substrate.

1. Introduction

The recent experimental demonstration of direct band gap in hexagonal Ge (*h*-Ge) and SiGe alloy **[1]** has opened new opportunities in the field of group-IV photonics **[2]–[4]**. While in its natural cubic phase Ge has an indirect band-gap, the hexagonal phase was predicted to have a direct band gap **[5]–[9]**. The hexagonal phases of Si and Ge were achieved in 2015 **[10]** and 2017 **[11],** respectively, thanks to the crystal transfer method. This method consists in the growth of III-V nanowires (NWs) with wurtzite (WZ) crystal structure, and the subsequent epitaxial growth of the group IV semiconductor (Si, Ge or an alloy) on the NW facets. As a result of the low lattice mismatch between GaAs and Ge or GaP and Si, the group IV semiconductor can adopt the hexagonal phase. Compared to *h*-Ge grown by metalorganic chemical vapor deposition (MOCVD) **[1]** molecular beam epitaxy (MBE) provides distinct advantages such as a high purity of the grown materials as well as the growth far from thermodynamic equilibrium, which are relevant to fabricate optimized quantum heterostructures for instance. Moreover, III-V MBE reactors can be easily equipped with Ge and/or Si evaporators.

In the pioneering work of Fadaly *et al.* [**1**] III-V NWs were grown on GaAs substrate with Au catalyst using MOCVD. While Au is probably the most popular catalyst for the NW growth using the vapor-liquid-solid (VLS) method, Au is known to induce defects and can diffuse into the semiconductor **[12], [13**]. An alternative solution consists in using the self-assisted method, where Au is replaced by Ga for the growth of GaAs NWs **[14], [15]**. Although replacing Au by Ga is promising to avoid the formation of defects, it was observed that self-assisted GaAs NWs exhibit mostly the zinc-blende (ZB) phase, which is detrimental to the fabrication of *h*-Ge. The occurrence of two crystal phases in GaAs NWs (WZ for Au catalyst and ZB for Ga catalyst) is closely related to the value of contact angle of the liquid catalyst during the VLS growth **[16]–[18],** and various strategies have been tested in order to control the synthesis of WZ in NW geometry **[19], [20].** Recently, we demonstrated the growth of a long segment of WZ GaAs using the self-assisted method by an accurate control of the group III **[21]** or group V flux **[22]** to ultimately reach a stationary state of the catalyst contact angle in the range inducing the WZ phase [**22**]. The facets of obtained WZ GaAs

NWs thus provide an ideal template for the epitaxial growth of *h*-Ge, in addition to their low lattice mismatch.

In this work, we demonstrate the growth of epitaxial *h*-Ge on the facets of self-assisted GaAs NWs by MBE. Our technique is gold catalyst-free and is realized directly on Si substrate. The as-grown NWs are thoroughly characterized using microscopic and spectroscopic techniques, and highlight the single-crystal quality of the Ge shell. This Au-free approach opens potential pathways for integrating *h*-Ge NWs in photonic devices such as lasers or near-infrared detectors **[23]**.

2. Growth condition to obtain hexagonal Ge

GaAs/Ge core-shell NWs were epitaxially grown on Si (111) substrate by MBE using the VLS mechanism. In order to obtain a long GaAs WZ segment as described in Figure 1(a) the crystal phase was tuned by a modification of the V/III ratio during the VLS growth. GaAs NWs were grown during 20 min with Ga and As_4 fluxes of 0.5 ML s^{-1} and 1.2 ML s^{-1}, respectively, corresponding to a V/III flux ratio 2.4 in order to obtain the ZB phase. To achieve the WZ phase, the V/III ratio was increased to 4.3 for 20 minutes (As_4 flux was increased to 2.1 ML s^{-1}). The growth of GaAs core was terminated by closing the Ga shutter in order to consume the droplet which is known to induce the formation of a short ZB segment at the NW tip. The growth was continuously monitored by *in situ* reflection high energy electron diffraction (RHEED), which characterizes the crystal structure of the samples during the growth, to obtain real time information of the growing crystal phase. Figure 1(b) and 1(c) illustrate the growing WZ phase of GaAs during 20 minutes, with the 4.3 V/III ratio. The intensity of the WZ spots on the RHEED increased after the 10^{th} minute of growth (Figure 1(b)) and the progressive intensity of WZ signal proved the growth of long hexagonal segment. The Ge shell was then epitaxially grown around the self-assisted GaAs core NWs. The Ge shell was grown at 400ºC for 30 min, which corresponds to a planar growth rate of 0.15 ML/s. RHEED images in Figure 1(d) and Figure 1(e) were recorded during the Ge growth after the 3^{rd} and 10^{th} minute, respectively. The RHEED signal did not change from Figure 1(c) to Figure 1(d) confirming that Ge followed the crystal structure of GaAs core. Figure 1(f) shows the scanning electron microscopy (SEM) image of the NWs, their

length is about 4.5 ± 1.2 μm and their diameter about 115 ± 10 nm. Thanks to this growth methodology, we expect NWs having a long hexagonal segment located near the tip as described in figure 1(a).

3. Structure and surface characterization of hexagonal Ge

High-resolution scanning transmission electron microscopy (STEM) imaging in high angle annular dark field (HAADF) imaging mode and elemental mapping using electron energy-loss spectroscopy (EELS) were performed to investigate the crystal structure and the epitaxial interface between GaAs and Ge. Several NWs were analyzed with the same results. The top part of the NWs can be easily identified from the Ge enrichment at the NW tip (see Figure S1 in the supplementary information section), which is a consequence of the Ge evaporator orientation (5° of incidence to the normal of the substrate). In agreement with the evolution of the RHEED pattern during the growth, cubic Ge is observed on ZB GaAs (see Figure S2 in the supplementary information section), while *h*-Ge is observed on WZ GaAs. As expected, the upper part of the NW exhibit a *h*-Ge / WZ GaAs segment of 500 nm. Figure 2(a) shows a STEM-HAADF low magnification image of typical NWs. Figure 2(b) shows a high-resolution STEM-HAADF image of this extended hexagonal segment. Interestingly, no extended defects **[24]** were identified, the low lattice mismatch between Ge and GaAs is probably accommodated by surface relaxation. Chemical mapping using EELS is superimposed on the high-resolution STEM-HAADF in Figure 2(b), and confirms the presence of a Ge shell, with a thickness of a few nm.

X-ray photoelectron spectroscopy (XPS) was used to investigate the presence of impurities and possible As contamination in the Ge shell. XPS measurements were carried out in a Prevac spectrometer equipped with a focused monochromatic X-ray source Al Kα (1486.6 eV), in a base pressure less than 10^{-9} mbar. The different spectra were recorded at 45° exit angle to maximize the signal coming from the side of the NWs. Following the method described previously, a thicker Ge shell was grown on GaAs NWs with a hexagonal segment estimated to 500 nm. The shell thickness was increased to 20 nm in order to maximize the signal from the Ge shell. After the growth, the sample was transferred in ultra-high vacuum to the XPS chamber, which is directly connected to the MBE reactor, for further analysis.

A large survey (shown in Figure 3(a)), O 1*s*, As 3*d*, Ge 3*d* and Ga 3*d* core level spectra of the sample were recorded and compared to a Ge substrate reference. The position and shape of Ge peaks from the NWs reproduce exactly the Ge peaks from the reference substrate, thus confirming the presence of Ge-Ge bonds. The Ge $3d_{5/2,3/2}$ multiplet, shown in Figure 3(b), was fitted using a spin-orbit splitting of 0.585 eV and an intensity ratio of 0.67, as expected statistically for *d* electrons and in agreement with literature **[25]**. The inelastic electron background was taken into account via a Shirley background correction. Ge 3*d* was found at 29.9 eV, corresponding to a slightly higher value than literature **[26]**.

The comparison between the two surveys reveals very weak signals coming from Ga 2*p* core level at about 1117 eV and from As Auger electrons around about 260 eV. Both are indicated in Figure 3(a). The amount of As, Ge and Ga at the extreme surface of the NWs can be easily compared in the Figure 3(b). The Ga 3*d* was barely visible in contrast to As 3*d*, suggesting a slight diffusion or contamination of As in Ge. By considering a homogeneous As_yGe overlayer in the NW, y is evaluated around 0.076 from the ratio of the 3*d* fitted peak areas times their cross sections. This amount might be overestimated as the fit allows to disentangle electrons from Ge metal loss of electrons and from As 3*d* core level, but does not to take into account the Shirley background. The presence of As in the Ge shell was already reported in ref [**1**] and attributed to As diffusion from the NW core due to high growth temperature (about 650°C). However, in our case the growth was performed at only 400°C, suggesting possible As contamination from the residual atmosphere in the MBE chamber during the Ge growth.

4. Conclusion & perspectives

In conclusion, we demonstrated the growth of *h*-Ge on self-assisted wurtzite GaAs segments in NW geometry. The core-shell NWs were grown directly on Si substrate using MBE. We succeeded to grow a long hexagonal segment of Ge with high structural quality that was confirmed by STEM. The XPS analysis reports the contamination of As in Ge, which strongly modify the electronic properties of *h*-Ge. Further optimization of the MBE growth conditions should be investigated in order to improve the quality of *h*-Ge.

Our results open the way to the fabrication of gold-free quantum heterostructures based on *h*-Ge and the realization of associated devices.

Methods

GaAs NWs were grown on p-doped Si(111) substrates using a solid-source MBE reactor. Before the introduction to the reactor, each Si substrate was cleaned with 5 min acetone and ethanol in an ultrasonic bath, and degassed at 200°C in ultra-high vacuum. Afterwards, the substrate was heated to 450°C and 1 monolayer (ML) of Ga was pre-deposited in 2 seconds at 0.5 ML.s^{-1}, quoted in units of equivalent growth rates of GaAs 2D layers measured by RHEED oscillations on a GaAs substrate **[27]**. The substrate temperature was increased to 580°C for the growth of GaAs core. GaAs NWs were grown with Ga and As_4 fluxes of 0.5 ML s^{-1} and 1.2 ML s^{-1}, respectively, corresponding to a V/III flux ratio 2.4. For the growth of WZ phase of GaAs, As_4 flux was increased to 2.1 ML s^{-1}, corresponding to a V/III flux ratio 4.3. The growth of GaAs core was terminated by closing the Ga shutter in order to consume the droplet.

GaAs core NWs were used as a template and were overgrown with Ge shell by opening the shutter of Ge cell. The samples were monitored *in situ* by RHEED to obtain real time information on the crystal structure of GaAs/Ge NWs. The NW morphology was characterized by SEM (Jeol JSM7401F). The transmission electron microscopy experiments were carried out in a Jeol JEM ARM200F Cold-FEG NeoARM, equipped with a last generation CEOS aberration-corrector (ASCOR) of the condenser lenses, a Gatan GIF Quantum, and operated at 200 kV. The characterized NWs were mechanically reported from the as-grown substrate to a lacey carbon TEM grid. The crystal phase was confirmed by high resolution STEM in high-angle annular dark field (HAADF) imaging mode. Elemental maps discriminating the core and shell were performed by electron energy-loss spectroscopy (EELS) in STEM mode using the spectrum imaging routine implemented in the Gatan GMS3 software. The maps were extracted after background removal and integration of the Ga-L_{23} and Ge-L_{23} edges. A dwell time of 200 ms/channel and a dispersion of 0.25 eV/channel were used for the maps in Figure 2 and Figure S1.

XPS measurements were carried out in a Prevac spectrometer equipped with a focused monochromatic X-ray source Al Kα (1486.6 eV), in a base pressure less than 10^{-9} mbar. The different spectra were recorded at 45° exit angle to maximize the signal coming from the side of the NWs. The energy calibration was checked with gold reference (Au 4*f* at 84(+/-0.1) eV) just before the experiment. A Ge substrate was used as a reference sample. The C1s signal is found negligible for all samples. There is no evidence for oxygen in the NWs, as expected from a growth and transfer under UHV.

Data availability

The data that support the findings of this study are available from the corresponding author upon reasonable request.

Supporting information

- HAADF-STEM image showing the top of the NW
- High-resolution STEM-HAADF images showing the different crystal structures

Acknowledgements

The authors thank the NanoLyon platform for access to the equipments and J. B. Goure for technical assistance. The authors acknowledge the French Agence Nationale de la Recherche (ANR) for funding under project BEEP (ANR-18-CE05-0017-01). This work was supported by the LABEX iMUST (ANR-10-LABX-0064) of Université de Lyon, within the program "Investissements d'Avenir" (ANR-11-IDEX-0007) operated by the French National Research Agency (ANR). The STEM work was performed at the consortium Lyon-St-Etienne de microscopie. The authors are grateful to Y. Lefkir and S. Reynaud for technical assistance using the Jeol NeoARM instrument. This project has received funding from the European Union's Horizon 2020 research and innovation programme under the Marie Skłodowska-Curie grant agreement No 801512.

Bibliography

[1] E. M. T. Fadaly *et al.*, 'Direct-bandgap emission from hexagonal Ge and SiGe alloys', *Nature*, vol. 580, no. 7802, pp. 205–209, Apr. 2020, doi: 10.1038/s41586-020-2150-y.

[2] D. de Matteis *et al.*, 'Probing Lattice Dynamics and Electronic Resonances in Hexagonal Ge and Si_xGe_{1-x} Alloys in Nanowires by Raman Spectroscopy', *ACS Nano*, vol. 14, no. 6, pp. 6845–6856, Jun. 2020, doi: 10.1021/acsnano.0c00762.
[3] R. Geiger, T. Zabel, and H. Sigg, 'Group IV Direct Band Gap Photonics: Methods, Challenges, and Opportunities', *Front. Mater.*, vol. 2, Jul. 2015, doi: 10.3389/fmats.2015.00052.
[4] L. Vivien, 'Silicon chips lighten up', *Nature*, vol. 528, no. 7583, pp. 483–484, Dec. 2015, doi: 10.1038/528483a.
[5] C. Raffy, J. Furthmüller, and F. Bechstedt, 'Properties of hexagonal polytypes of group-IV elements from first-principles calculations', *Phys. Rev. B*, vol. 66, no. 7, p. 075201, Aug. 2002, doi: 10.1103/PhysRevB.66.075201.
[6] T. Kaewmaraya, L. Vincent, and M. Amato, 'Accurate Estimation of Band Offsets in Group IV Polytype Junctions: A First-Principles Study', *J. Phys. Chem. C*, vol. 121, no. 10, pp. 5820–5828, Mar. 2017, doi: 10.1021/acs.jpcc.6b12782.
[7] C. Rödl, J. Furthmüller, J. R. Suckert, V. Armuzza, F. Bechstedt, and S. Botti, 'Accurate electronic and optical properties of hexagonal germanium for optoelectronic applications', *Phys. Rev. Materials*, vol. 3, no. 3, p. 034602, Mar. 2019, doi: 10.1103/PhysRevMaterials.3.034602.
[8] E. Scalise *et al.*, 'Thermodynamic driving force in the formation of hexagonal-diamond Si and Ge nanowires', *Applied Surface Science*, vol. 545, p. 148948, Apr. 2021, doi: 10.1016/j.apsusc.2021.148948.
[9] X. Cartoixà, M. Palummo, H. I. T. Hauge, E. P. A. M. Bakkers, and R. Rurali, 'Optical Emission in Hexagonal SiGe Nanowires', *Nano Lett.*, vol. 17, no. 8, pp. 4753–4758, Aug. 2017, doi: 10.1021/acs.nanolett.7b01441.
[10] H. I. T. Hauge *et al.*, 'Hexagonal Silicon Realized', *Nano Lett.*, vol. 15, no. 9, pp. 5855–5860, Sep. 2015, doi: 10.1021/acs.nanolett.5b01939.
[11] H. I. T. Hauge, S. Conesa-Boj, M. A. Verheijen, S. Koelling, and E. P. A. M. Bakkers, 'Single-Crystalline Hexagonal Silicon–Germanium', *Nano Lett.*, vol. 17, no. 1, pp. 85–90, Jan. 2017, doi: 10.1021/acs.nanolett.6b03488.
[12] T. Xu, J. Sulerzycki, J. Nys, G. Patriarche, B. Grandidier, and D. Stiévenard, 'Synthesis of long group IV semiconductor nanowires by molecular beam epitaxy', *Nanoscale Res Lett*, vol. 6, no. 1, p. 113, 2011, doi: 10.1186/1556-276X-6-113.
[13] J. B. Hannon, S. Kodambaka, F. M. Ross, and R. M. Tromp, 'The influence of the surface migration of gold on the growth of silicon nanowires', *Nature*, vol. 440, no. 7080, pp. 69–71, Mar. 2006, doi: 10.1038/nature04574.
[14] A. Fontcuberta i Morral, D. Spirkoska, J. Arbiol, M. Heigoldt, J. R. Morante, and G. Abstreiter, 'Prismatic Quantum Heterostructures Synthesized on Molecular-Beam Epitaxy GaAs Nanowires', *Small*, vol. 4, no. 7, pp. 899–903, Jul. 2008, doi: 10.1002/smll.200701091.
[15] M. M. Jansen *et al.*, 'Phase-Pure Wurtzite GaAs Nanowires Grown by Self-Catalyzed Selective Area Molecular Beam Epitaxy for Advanced Laser Devices and Quantum Disks', *ACS Appl. Nano Mater.*, vol. 3, no. 11, pp. 11037–11047, Nov. 2020, doi: 10.1021/acsanm.0c02241.
[16] F. Glas, J.-C. Harmand, and G. Patriarche, 'Why Does Wurtzite Form in Nanowires of III-V Zinc Blende Semiconductors?', *Phys. Rev. Lett.*, vol. 99, no. 14, p. 146101, Oct. 2007, doi: 10.1103/PhysRevLett.99.146101.
[17] V. G. Dubrovskii, W. Kim, V. Piazza, L. Güniat, and A. Fontcuberta i Morral, 'Simultaneous Selective Area Growth of Wurtzite and Zincblende Self-Catalyzed GaAs Nanowires on Silicon', *Nano Lett.*, vol. 21, no. 7, pp. 3139–3145, Apr. 2021, doi: 10.1021/acs.nanolett.1c00349.
[18] F. Panciera *et al.*, 'Phase Selection in Self-catalyzed GaAs Nanowires', *Nano Lett.*, vol. 20, no. 3, pp. 1669–1675, Mar. 2020, doi: 10.1021/acs.nanolett.9b04808.
[19] W. Kim *et al.*, 'Bistability of Contact Angle and Its Role in Achieving Quantum-Thin Self-Assisted GaAs nanowires', *Nano Lett.*, vol. 18, no. 1, pp. 49–57, Jan. 2018, doi: 10.1021/acs.nanolett.7b03126.

[20] V. G. Dubrovskii, G. E. Cirlin, N. V. Sibirev, F. Jabeen, J. C. Harmand, and P. Werner, 'New Mode of Vapor−Liquid−Solid Nanowire Growth', *Nano Lett.*, vol. 11, no. 3, pp. 1247–1253, Mar. 2011, doi: 10.1021/nl104238d.
[21] T. Dursap *et al.*, 'Crystal phase engineering of self-catalyzed GaAs nanowires using a RHEED diagram', *Nanoscale Adv.*, vol. 2, no. 5, pp. 2127–2134, 2020, doi: 10.1039/D0NA00273A.
[22] T. Dursap *et al.*, 'Wurtzite phase control for self-assisted GaAs nanowires grown by molecular beam epitaxy', *Nanotechnology*, vol. 32, no. 15, p. 155602, Apr. 2021, doi: 10.1088/1361-6528/abda75.
[23] I. V. Ilkiv *et al.*, 'Formation of Hexagonal Ge Stripes on the Side Facets of AlGaAs Nanowires: Implications for Near-Infrared Detectors', *ACS Appl. Nano Mater.*, p. acsanm.1c01266, Jul. 2021, doi: 10.1021/acsanm.1c01266.
[24] E. M. T. Fadaly *et al.*, 'Unveiling Planar Defects in Hexagonal Group IV Materials', *Nano Lett.*, vol. 21, no. 8, pp. 3619–3625, Apr. 2021, doi: 10.1021/acs.nanolett.1c00683.
[25] M. El Kazzi *et al.*, 'Ge/SrTiO 3 (001) interface probed by soft x-ray synchrotron-radiation time-resolved photoemission', *Phys. Rev. B*, vol. 85, no. 7, p. 075317, Feb. 2012, doi: 10.1103/PhysRevB.85.075317.
[26] M. K. Hudait *et al.*, '*In situ* grown Ge in an arsenic-free environment for GaAs/Ge/GaAs heterostructures on off-oriented (100) GaAs substrates using molecular beam epitaxy', *Journal of Vacuum Science & Technology B, Nanotechnology and Microelectronics: Materials, Processing, Measurement, and Phenomena*, vol. 30, no. 5, p. 051205, Sep. 2012, doi: 10.1116/1.4742904.
[27] D. Rudolph *et al.*, 'Direct Observation of a Noncatalytic Growth Regime for GaAs Nanowires', *Nano Lett.*, vol. 11, no. 9, pp. 3848–3854, Sep. 2011, doi: 10.1021/nl2019382.

Figures

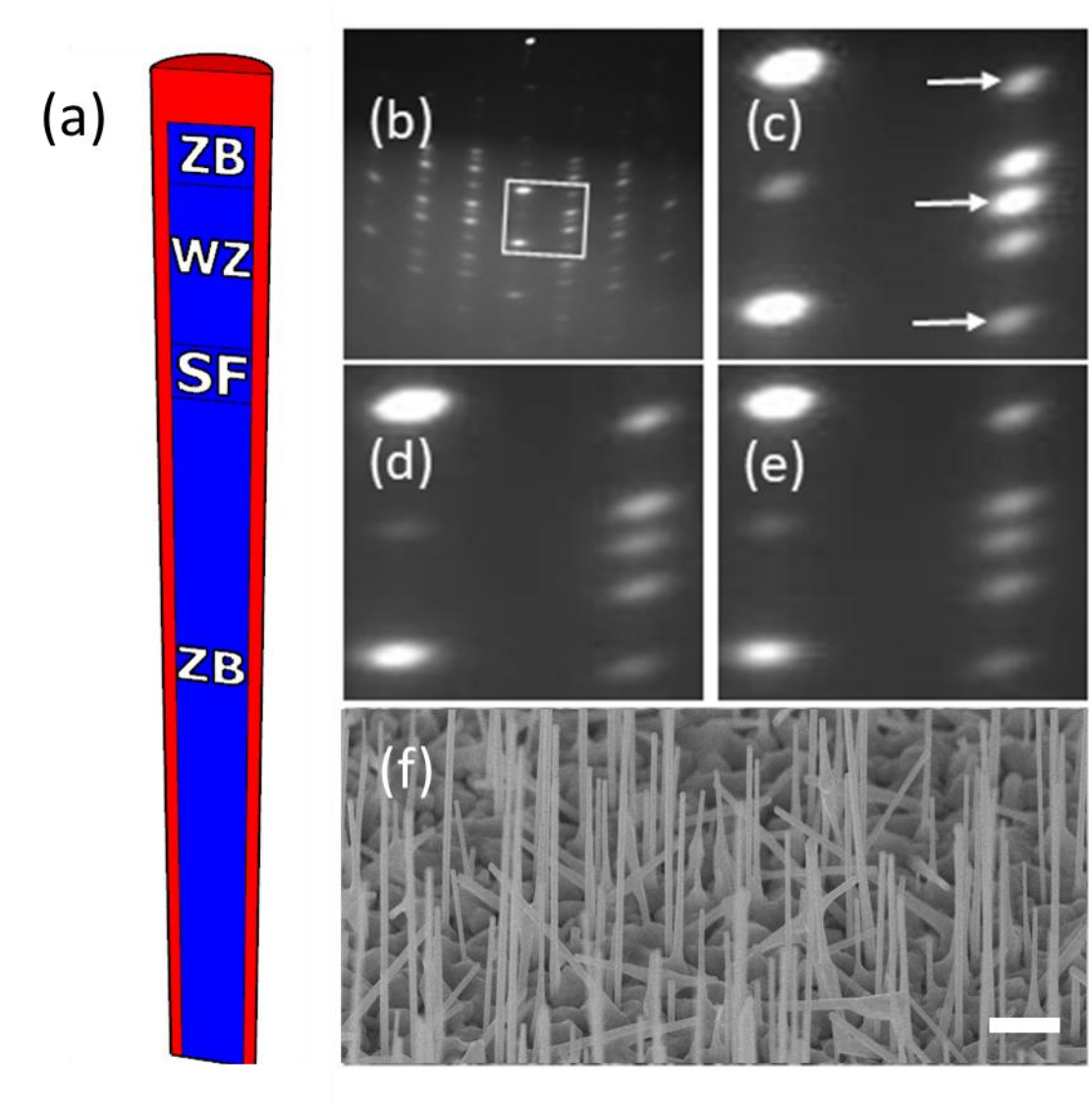

Figure 1: (a) Schematic of a GaAs core (blue) - Ge shell (red) NW with controlled crystal phase: wurtzite (WZ), zinc-blende (ZB), with a region of stacking faults (SF). The samples were monitored *in situ* by RHEED to obtain real time information on the crystal structure of GaAs/Ge NWs. RHEED patterns recorded along the [1-10] azimuth during the growth of WZ GaAs at (b) 29 min (c) 35 min and of hexagonal Ge at (d) 3 min (e) 10 min. The WZ spots are highlighted with the white arrows. (f) 45° tilt SEM image (secondary electron contrast) showing the GaAs/Ge NWs. The scale bar is 1 μm.

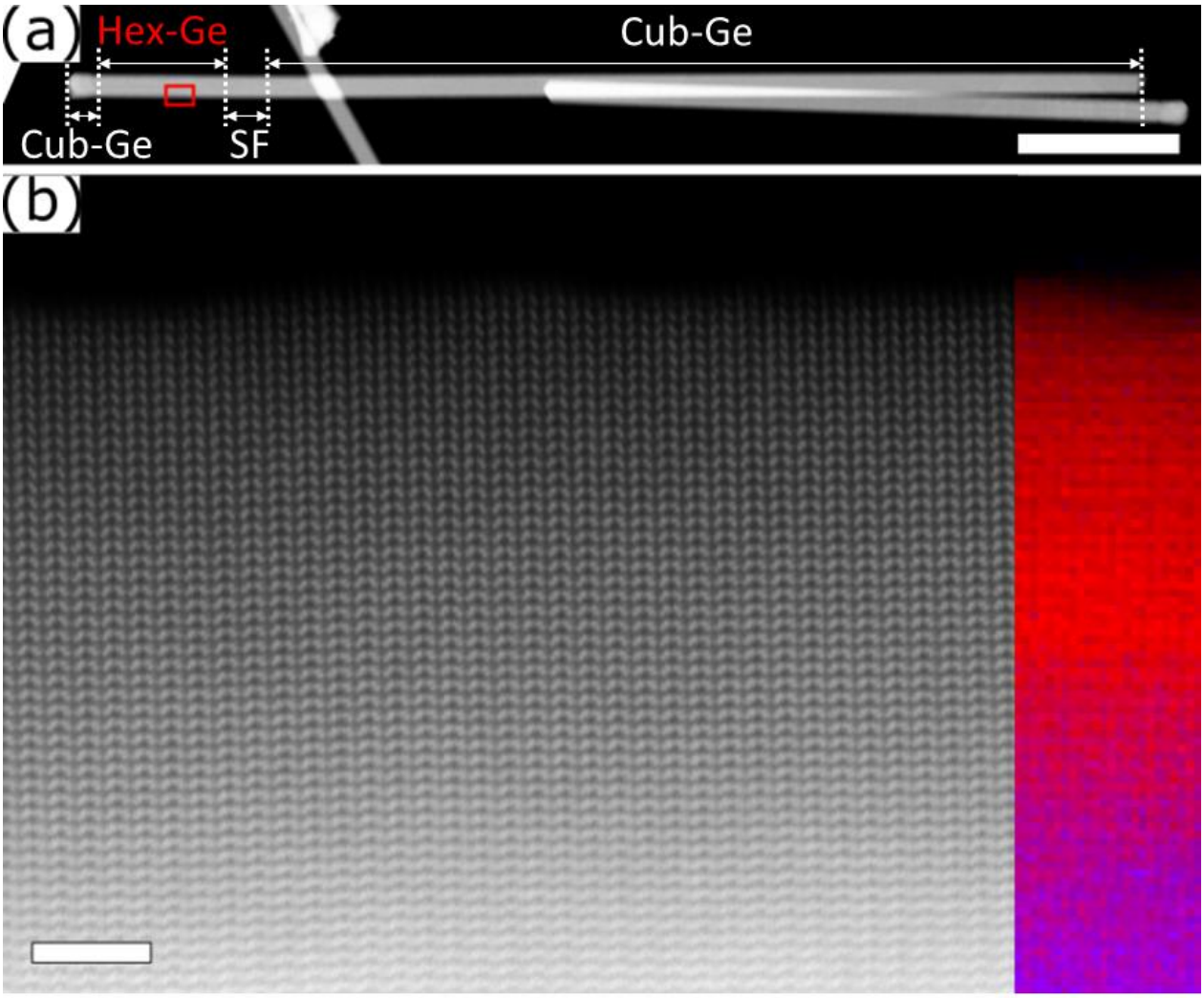

Figure 2: (a) STEM-HAADF overview of a NW. Scale bar is 500 nm. (b) High resolution STEM-HAADF image of the WZ structure with a superimposed Ga (blue) and Ge (red) maps extracted from multiple linear least square (MLLS) fitting. Scale bar is 2 nm. The region shown in (b) is highlighted by a red rectangle in (a). The EELS map of the Ga-L_{23} (blue) and the Ge-L_{23} (red) edges is superimposed.

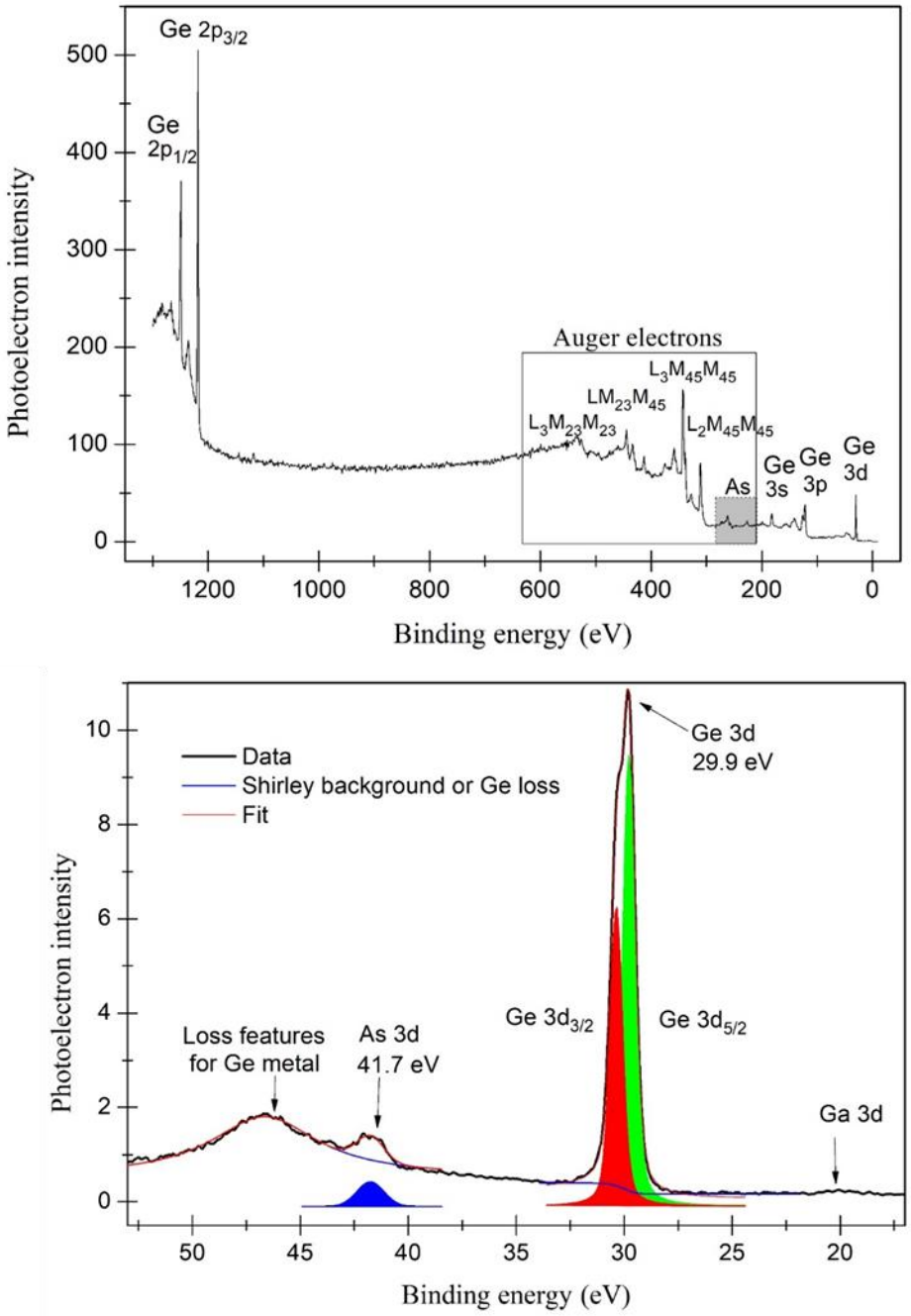

Figure 3: XPS spectra of GaAs/Ge nanowires (a) full range survey spectrum (b) Ge 3*d* core level spectrum. The energy calibration was checked with gold reference (Au 4f at 84(+/-0.1) eV) just before the experiment. A Ge substrate was used as a reference sample. The C1s signal is found negligible for all samples. There is no evidence for oxygen in the NWs, as expected from a growth and transfer under UHV.

For Table of Contents Only

Hexagonal Ge grown by molecular beam epitaxy on self-assisted GaAs nanowires

Iuliia Dudko[1,2,3], Thomas Dursap[1], Anne D. Lamirand[1], Claude Botella[1], Philippe Regreny[1], Alexandre Danescu[1], Solène Brottet[1], Matthieu Bugnet[2], Sumeet Walia[2,3], Nicolas Chauvin[1], José Penuelas[1]*

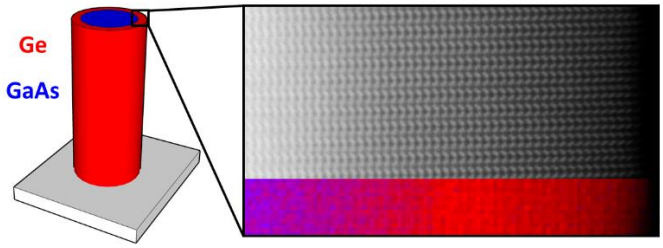

We demonstrate the possibility to use Molecular Beam Epitaxy to obtain hexagonal germanium, moreover our approach is gold free and integrated on GaAs on silicon substrate.